Earth Planet. Sci. Lett. 623 (2023) 118434

Contents lists available at ScienceDirect

Earth and Planetary Science Letters

journal homepage: www.elsevier.com/locate/epsl

Uranium isotopes as tracers of serpentinite weathering

Frank J. Pavia [a,*], Emily H.G. Cooperdock [b], Juan Carlos de Obeso [c,d], Kenneth W.W. Sims [e], François L.H. Tissot [f], Frieder Klein [g]

[a] Division of Geological and Planetary Sciences, California Institute of Technology, United States
[b] University of Southern California, Department of Earth Sciences, Los Angeles, CA 90089, United States
[c] University of Calgary, Department of Geosciences, Canada
[d] University of Utah, Department of Geology and Geophysics, United States
[e] Wyoming High Precision Isotope Laboratory, Department of Geology and Geophysics, University of Wyoming, Laramie, WY, 82071, United States
[f] The Isotoparium, Division of Geological and Planetary Sciences, California Institute of Technology, United States
[g] Woods Hole Oceanographic Institution, Department of Marine Chemistry and Geochemistry, Woods Hole, MA, 02543, United States

ARTICLE INFO

Keywords:
Serpentinite
Weathering
Uranium isotopes
Isotope geochemistry

ABSTRACT

The aqueous alteration of mantle rocks is considered to play a key role in Earth's global biogeochemical cycling. Uranium enrichment in fluid-altered mantle rocks is a common feature that may reflect redox state or fluid source, but it remains unclear when, why, and how uranium is mobilized within these systems. In this study we use uranium (U) isotopes ($^{234}U/^{238}U$ and $^{238}U/^{235}U$ ratios) to deduce the timing, mobilization processes, and fluid sources responsible for weathering of subaerial and submarine serpentinites. We find that complex post-formation weathering processes continue to perturb serpentinite U isotope compositions and U concentrations long after initial serpentinization. Enriched $^{234}U/^{238}U$ ratios in dredged seafloor serpentinites require recent (<1.5 Myr) uptake of U, likely from derived from chemically evolved seawater that has circulated through igneous basement rocks. In contrast, depleted and variable $^{234}U/^{238}U$ ratios in a terrestrial serpentinite across <30 cm spatial scales from the Wadi Fins outcrop in the Samail Ophiolite, Oman, indicate alpha recoil effects, with differences in these ratios reflecting different grain sizes or shapes of U-hosting minerals in different weathering zones. Both seafloor and Wadi Fins serpentinites have $^{238}U/^{235}U$ ratios significantly different from seawater and mid-ocean ridge basalts, reflecting different initial protolith composition and/or overprinting of $^{238}U/^{235}U$ ratios during weathering. Using $^{238}U/^{235}U$ and U concentrations we calculate the isotopic composition of evolved fluids weathering the serpentinites at both localities. We also use $^{234}U/^{238}U$ and models of alpha recoil to determine the grain sizes of minerals hosting U from samples at Wadi Fins. Our results suggest that U isotopic compositions and concentrations are sensitive to post-serpentinization weathering processes in subaerial and submarine environments. The U isotopic composition of abyssal serpentinites is set by seawater that has chemically evolved during flow through basement rocks, questioning the utility of weathered serpentinites as an archive of paleo-seawater U isotope compositions, as well as other fluid-mobile elements modified during crustal fluid flow.

1. Introduction

The process of serpentinization, where aqueous fluids alter primary minerals in peridotite to form serpentine and other secondary phases, makes serpentinite a key reservoir in the global cycles of water, carbon dioxide, and fluid-mobile elements in the solid Earth. Because serpentinite has formed throughout Earth's history, ancient serpentinites have been used as proxies for fluid-rock interactions, changes in rheology, and ancient microbial habitats on early Earth (D'Andres et al., 2019; Pope et al., 2012; Scott et al., 2017) However, serpentinite exposed to seawater or meteoric fluids is susceptible to weathering by open-system alteration at low-temperatures (Beinlich et al., 2018; Klein et al., 2020; Mervine et al., 2015; Mervine et al., 2014; Snow and Dick, 1995). Seafloor weathering of oceanic serpentinite can modify its mineralogy, chemical composition, and physical properties (Klein et al., 2017). Continental weathering of serpentinite has been linked to Mg isotope fractionation, Ni enrichment, and CO_2 sequestration (Beinlich et al., 2018; Mervine et al., 2015; Mervine et al., 2014; de Obeso et al., 2021;

* Corresponding author.
E-mail address: fjpavia@caltech.edu (F.J. Pavia).

https://doi.org/10.1016/j.epsl.2023.118434
Received 27 February 2023; Received in revised form 3 October 2023; Accepted 5 October 2023

Power et al., 2013).

Despite its prevalence, many aspects of serpentinite weathering remain poorly understood, including the fluid sources, timescales of weathering, and redox conditions. Knowledge of which elements are mobile and under what conditions becomes particularly important for serpentinite systems used as geochemical proxies (D'Andres et al., 2019), as well as systems used to understand fluid sources of elements delivered to the mantle by subduction (Kendrick et al., 2011). Specifically, how do fluids impart their chemistry into serpentinite and how does subsequent weathering modify that signal?

Here we explore the impact of weathering processes on uranium concentrations [U] and isotope ratios in serpentinite systems. Seafloor serpentinite exhibits [U] enrichment by up to 1000x compared to unaltered mantle peridotite (Kodolányi et al., 2011; Niu, 2004; Paulick et al., 2006). Uranium enrichment in serpentinite is generally attributed to interaction with seawater, which is a well-mixed U source (Chen et al., 1986). Recent work documents a similar range of U enrichment in a subaerially exposed serpentinite (de Obeso and Kelemen, 2020). The mechanism for U enrichment, where U is hosted, and the timing of uptake during serpentinization and post-serpentinization weathering are not well known, particularly in regard to how they vary across different geologic settings (Kodolányi et al., 2011).

Uranium isotopes provide a potential toolkit for evaluating serpentinite formation conditions and weathering. The 'stable' isotope ratios of $^{238}U/^{235}U$ are fractionated during U redox transformations between U (VI) and U(IV), with higher $^{238}U/^{235}U$ ratios found in solids formed under reducing conditions (Andersen et al., 2017; Stirling et al., 2007; Tissot and Dauphas, 2015; Weyer et al., 2008). The radiogenic U isotope ratios, $^{234}U/^{238}U$, deviate from secular equilibrium (activity ratio of 1) due to either U addition from fluid sources with high $^{234}U/^{238}U$ ratios, or due to preferential removal of ^{234}U relative to ^{238}U during rock weathering (DePaolo et al., 2006; Fleischer, 1980; Kigoshi, 1971).

In this study, we present $^{238}U/^{235}U$, $^{234}U/^{238}U$, and U concentrations in a suite of oceanic and continental serpentinites and we use these measurements to assess the fluid histories and weathering dynamics of U. To our knowledge, these are the first published measurements of uranium isotopes in serpentinites. An initial motivation of our study was to determine whether serpentinites record the $^{238}U/^{235}U$ ratio of seawater, thus opening the door to their use as archives of past $^{238}U/^{235}U$ variations in the deep ocean, which reflect the extent of seafloor anoxia. We find that serpentinite $^{234}U/^{238}U$ ratios deviate significantly from secular equilibrium in our study sites, and that these $^{234}U/^{238}U$ variations correlate strongly with $^{238}U/^{235}U$. Our findings provide new constraints on the timescales and fluid sources of weathering in submarine and subaerial environments and suggest that serpentinites likely do not record the unaltered $^{238}U/^{235}U$ ratio of seawater.

2. Background and methods

2.1. Sample descriptions and geological context

Well-characterized samples from oceanic and continental settings were selected that had previously published petrology and geochemistry.

2.1.1. Dredged seafloor serpentinites

Oceanic samples were dredged from the Southwest Indian Ridge, South American-Antarctic Ridge, and Central Mid-Atlantic Ridge. Sample CH35 18–287 is a strongly serpentinized and weathered peridotite protomylonite dredged north of the St. Paul's Rocks archipelago. Samples Vulc-5 35–37 and Vulc-5 41–29 are partially serpentinized and weathered peridotites from the Bullard Fracture Zone and the Vulcan Fracture Zone, respectively (American Antarctic Ridge). Sample IO 11–76 60–171B is a completely serpentinized and weathered peridotite that was dredged at the Islas Orcadas Fracture Zone (Southwest Indian Ridge). Sample KN162–9 58–23 is a strongly serpentinized and weathered peridotite that was dredged at Oblique Spreading Center on the Southwest Indian Ridge. Dredged samples show brown staining due to the formation of hematite and goethite at the expense of magnetite whereas none of these samples contain brucite, consistent with prolonged exposure to seawater at or near the seafloor (Klein et al., 2020). The occurrence of relict magnetite in these samples suggests that the temperature of serpentinization likely exceeded 200 °C (Klein et al., 2013; Klein et al., 2014). Approximate seafloor ages for these samples range from 1.5 to 11.4 Ma (Table 1). For additional sample-specific information see Dick (1989) and Klein et al. (2020).

2.1.2. Wadi fins continental serpentinites

Continental samples came from a peridotite outcrop in Wadi Fins (Samail Ophiolite, Sultanate of Oman (22.891611 ºN, 59.169060 ºE). These samples were collected in the bottom of a deep canyon where serpentinized peridotite is exposed below an unconformable contact with Cretaceous limestone (de Obeso and Kelemen, 2020). Samples were taken from an outcrop that exhibits concentric alteration patterns characterized by sharp oxidation fronts and mineralogical changes over length-scales of one to thirty centimeters, with cross-cutting calcite and serpentine veins (Fig. 1). Three samples (OM15–5, OM15–6, OM15–7) were collected within 5–10 m of each other, each one targeting an independent concentric alteration pattern, totaling three distinct alteration profiles. Each of these profiles was subdivided into three sub-samples, labeled core, green, and red zones (Fig. 1). Subsamples were analyzed from a total of one core zone (OM15–6), two green zones (OM15–6, OM15–7) and three red zones (OM15–5, OM15–6, OM15–7) (Table 1).

Here we provide a brief overview of the characteristics and hypothesized formation histories of these zones based on the findings in de Obeso and Kelemen (2020), where a full accounting of these alteration zones can be found. Core zones are the least altered, consisting of partially serpentinized peridotite with low [U] and evidence of reducing formation conditions inferred from the presence of sulfide mineral assemblages and low Fe^{3+}/Fe^{tot}. Green zones are nearly completely serpentinized, with MgO and FeO depletions and 10x Sr, Rb, and U enrichments relative to the core zones. Sulfides present in the green zones have low metal to sulfur ratios, which alongside the high Sr, Rb, and U suggest formation under more oxidizing conditions and higher water/rock ratios than the core zones. Red zones are more oxidized than either core or green, with goethite present in bulk rock powder XRD analyses, significant enrichment in FeO, high Fe^{3+}/Fe^{tot}, similar Sr and Rb enrichments as the green zones, but with [U] concentrations 10x higher than green zones. Calcite veins in Wadi Fins are typically associated with the red zones, but smaller veins extend into the core and green zones, as well.

The proposed geologic history of the Wadi Fins samples is that serpentinization of the peridotite began during the Late Cretaceous. Alteration zones formed as seawater percolated through overlying carbonates and through the peridotite, serpentinizing primary minerals, and mobilizing Fe and Mg between core, green, and red zones during

Table 1
Dredge Serpentinite Sample Name, Location, and Approximate Seafloor Age.

Sample Name	Ridge Location	Latitude	Longitude	Seafloor Age (Ma) (Müller et al., 2008)
CHN35 18–287	St Paul's Rocks	00 56.0′ N	29 20.0′ W	4.2
VULC-5 41–29	Vulcan FZ SAAR	59 05.21′ S	16 48.46′ W	1.5
IO11–76 60–171b	Islas Orcadas FZ SWIR	54 02.7′ S	6 29.2′ E	1.5
KN162–9 58–23	SWIR Oblique SC	52 06.4′ S	13 43.9′ E	3.8
VULC-5 35–37	Bullard FZ SAAR	57 56.97′ S	7 48.73′ W	11.4

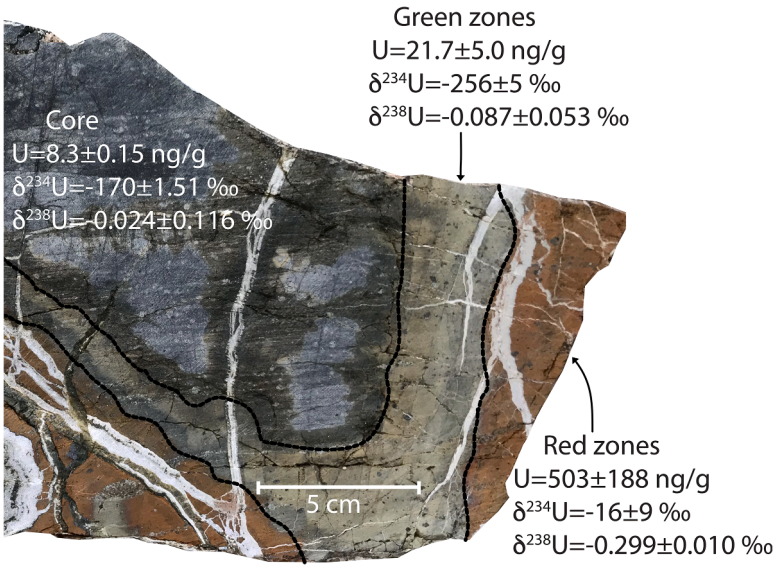

Fig. 1. Sample OM15–7 from Wadi Fins showing the three alteration zones discussed in this paper, as well as the average U concentrations, δ^{234}U values, and δ^{238}U values measured for these zones. Stippled lines demarcate the core, green, and red zones analyzed in this study.

weathering (see Figure 12 in de Obeso and Kelemen, 2020). The behavior of Fe during serpentinization and weathering is critical because it largely controls the potential for oxidation–reduction reactions (Scott et al., 2017). Magnetite grains in carbonate veins that cross-cut the red and green zones were dated to be 15 ± 4 Ma by (U-Th)/He chronometry, suggesting that the formation of the alteration zones was complete by ~15 Ma (Cooperdock et al., 2020).

2.2. Analytical methods

Prior to crushing, calcite veins were removed from the Wadi Fins samples to provide pure lithological separates from each zone. We measured the calcium carbonate content of these Wadi Fins separates as a check on the efficacy of the vein removal. Sample powder aliquots were loaded into AutoMate vials, which were subsequently evacuated and acidified using 10% phosphoric acid. The CO_2 produced by acidification was measured by a G2131-I Picarro cavity ringdown spectrometer coupled to an AutoMate autosampler at University of Southern California, following established methods (Dong et al., 2022). We note that this method only dissolves calcium carbonate, not dolomite or magnesite, which require higher temperatures and stronger acids to dissolve (Yager et al., 2017).

X-ray diffraction (XRD) analyses were performed on both dredged serpentinite and Wadi Fins samples. Oceanic serpentinite powders were analyzed at Woods Hole Oceanographic Institution using a Phillips Analytical PW1830 instrument. XRD of Wadi Fins sample powders were analyzed at Lamont-Doherty Earth Observatory, using an Olympus Terra XRD and Match! software (de Obeso and Kelemen, 2020). Fe^{3+}/Fe^{tot} was determined by mass balance using X-ray fluorescence analysis for oceanic samples at the Peter Hooper GeoAnalytical Lab at Washington State University and using ICP-OES analyses of Fe_2O_3 for Wadi Fins samples (de Obeso and Kelemen, 2020), together with FeO analyzed by titration for both sample suites. Loss on ignition was measured by heating to 900 °C for oceanic serpentinites and 950 °C for Wadi Fins. Thorium (Th), rubidium (Rb), and cesium (Cs) concentrations for submarine samples were determined by ICP-MS at the Washington State University GeoAnalytical Lab. Wadi Fins Th, Rb, and Cs were previously reported (de Obeso and Kelemen, 2020) and were measured on a VG PlasmaQuad ExCell ICP-MS.

Sample processing and U isotope analyses of both dredged and Wadi Fins serpentinites were performed at the Isotoparium (Caltech) following previously published protocols (Tissot and Dauphas, 2015). In brief, 100–430 mg of sample powders were digested in HF-HNO_3 mixtures, checked for their U concentrations via an iCAP RQ ICP-MS, and spiked with the IRMM-3636 ^{233}U-^{236}U double spike to achieve a spike/sample U ratio of ~ 3% (Tissot et al., 2019). Uranium purification was done using two successive separations on U/Teva resin and U isotopes were measured on a Thermo Neptune Plus MC-ICPMS. We calculated U isotope ratios and concentrations using a double spike inversion protocol (Tissot and Dauphas, 2015).

The $^{238}U/^{235}U$ ratios are reported as δ^{238}U values in units of permil relative to the U standard CRM-112a ($^{238}U/^{235}U = 137.837$ (Richter et al., 2010); also named SRM960 or NBL112-a; CRM-145 for the solution form):

$$\delta^{238}\mathrm{U} = \left[\frac{^{238}U/^{235}U_{sample}}{^{238}U/^{235}U_{standard}} - 1\right] \times 1000.$$

The $^{234}U/^{238}U$ ratios are expressed relative to secular equilibrium as:

$$\delta^{234}\mathrm{U}_{\mathrm{sec}} = \left[\frac{^{234}U/^{238}U_{sample}}{^{234}U/^{238}U_{S.E.}} - 1\right] \times 1000,$$

where $(^{234}U/^{238}U)_{S.E.}$ is the atomic ratio at secular equilibrium and is equal to the ratio of the decay constants of ^{238}U and ^{234}U, $\lambda_{238}/\lambda_{234} = (1.5513 \times 10^{-10})/(2.8220 \times 10^{-6}) = 5.497 \times 10^{-5}$ (Cheng et al., 2013).

Uncertainties are reported as the 95% confidence interval and calculated as the 2-sigma standard deviation of CRM-145 standard solutions bracketed by themselves for a given session divided by the square root of the number of sample replicates analyzed. To monitor accuracy, we measured three full procedural replicates of the USGS reference material BCR-2. These gave average δ^{234}U values of -0.113 ± 0.240 ‰, within error of $\delta^{234}U = 0$ ‰ (Table S1) and consistent with historical results for BCR-2 (Cheng et al., 2013; Matthews et al., 2010; Tissot et al., 2018) but about 0.6 ‰ lower than the recent highly precise values determined by Kipp et al. (2022). The δ^{238}U values of the three BCR-2 replicates we measured were -0.261 ± 0.018 ‰, within error of the average literature value of -0.262 ± 0.004 ‰ ($n = 36$) (data available taken from the uranium isotope database (Li and Tissot, 2023)).

3. Results

The seafloor samples experienced varying degrees of serpentinization and weathering: CHN35 18–287 is a partially serpentinized peridotite, IO11–76 60–171b is a serpentinized peridotite with its outer

weathering rind removed. While all abyssal samples showed visual evidence of moderate to pervasive weathering, none of them contain brucite (Klein et al., 2020). Seafloor serpentinites analyzed in this study with XRD are all primarily composed of serpentine (lizardite) with minor magnetite and in most cases small amount of relict orthopyroxene and olivine. In addition samples VULC-5 41–29 and CHN35 18–287 contain small amounts of dolomite and tremolite, respectively.

The mineralogy of Wadi Fins samples shows increasing degrees of serpentinization in sequential order of the core being the least altered, followed by green zones, with red zones being the most altered. Core zones contain primary minerals such as olivine, pyroxene, and spinel in addition to serpentine. Green zones are dominated by lizardite, and clay minerals such as diopside and stevensite. Red zones are primarily lizardite and stevensite with intergrown goethite. More details on the trace mineralogy of Wadi Fins samples can be found in de Obeso and Kelemen (2020).

Fluid-mobile element (FME) concentrations (Rb, Cs) as well as ratios to immobile elements (Rb/Th, Cs/Th) show enrichments above depleted mantle values in both Wadi Fins and abyssal samples (Table S1), with the exception of the Wadi Fins core sample which does not show significant FME enrichment.

The oceanic samples have [U] ranging from 291 to 694 ng/g. One oceanic sample (CHN35 18–287) has δ^{234}U of 71‰, roughly halfway between the secular equilibrium value of 0 ‰ and the seawater value of 145.55 ‰ (Kipp et al., 2022). The δ^{238}U of CHN35 18–287 is −0.383 ± 0.055 ‰, within error of the seawater δ^{238}U of −0.379 ± 0.023 ‰ (Kipp et al., 2022). The other four oceanic serpentinites have δ^{234}U significantly higher than seawater, with values ranging from 281.1 to 400 ‰ (Fig. 2). These four other oceanic serpentinites also have δ^{238}U that are isotopically light compared to seawater, with values ranging from −0.645 to −0.575 ‰ (Fig. 2).

The [U], δ^{234}U, and δ^{238}U in the Wadi Fins rocks show variability corresponding to the different alteration zones (Figs. 1, 2). The core sample (black square, Fig. 2) has [U] of 8.3 ± 0.15 ng/g, δ^{234}U of −170.1 ± 1.51 ‰, and a δ^{238}U value of −0.024 ± 0.116 ‰. Green zone samples have higher [U] averaging 21.7 ± 5 ng/g but lower average δ^{234}U values of -256 ± 5‰, and marginally lower average δ^{238}U of −0.087 ± 0.053 whereas red zone samples have the highest [U] and δ^{234}U values amongst the continental samples; 503 ± 188 ng/g and -16 ± 9 ‰, respectively, and lowest average δ^{238}U of −0.299 ± 0.010 ‰ (Fig. 1) (Kipp et al., 2022).

Both sample suites have non-secular equilibrium δ^{234}U compositions (i.e., significantly offset from δ^{234}U of 0 ‰, Fig. 2). The δ^{234}U range of our samples, which spans several hundred ‰, is far larger than can be explained by stable isotope fractionation, which could drive a maximum fractionation of <2 ‰ for δ^{234}U for the 1 ‰ observed range of ^{238}U/^{235}U observed in this study (Tissot and Dauphas, 2015). Our data reveal a systematic difference between the submarine and subaerial sample suites, where the submarine samples dredged from multiple seafloor localities have exclusively positive δ^{234}U and the subaerial samples from Wadi Fins have exclusively negative δ^{234}U. The δ^{238}U values of both sample suites also show systematic differences both within and from each other. Continental samples have decreasing δ^{238}U from core to green to red zones, while oceanic samples have δ^{238}U values that are depleted relative to the continental samples, and with one exception are 0.2–0.25 ‰ lower than seawater. We focus our discussion on unraveling the processes that changed the U isotopic composition of the studied samples.

4. Discussion

4.1. Alteration of U isotope ratios in submarine serpentinites by weathering

The seafloor serpentinite samples come from different localities and ridge systems. High δ^{234}U and low δ^{238}U values (Fig. 2) suggest U addition from a δ^{234}U enriched and δ^{238}U depleted fluid, which we interpret as resulting from seafloor weathering. The idea that seafloor serpentinization and subsequent weathering adds U is based on observed U enrichments in dredged and drilled oceanic serpentinites from distinct tectonic environments (Deschamps et al., 2013; Kodolányi et al., 2011; Peters et al., 2017). While it is generally assumed that the source for U enrichment is seawater, when the U addition occurs and where the U is hosted are still unknown, especially since it has been

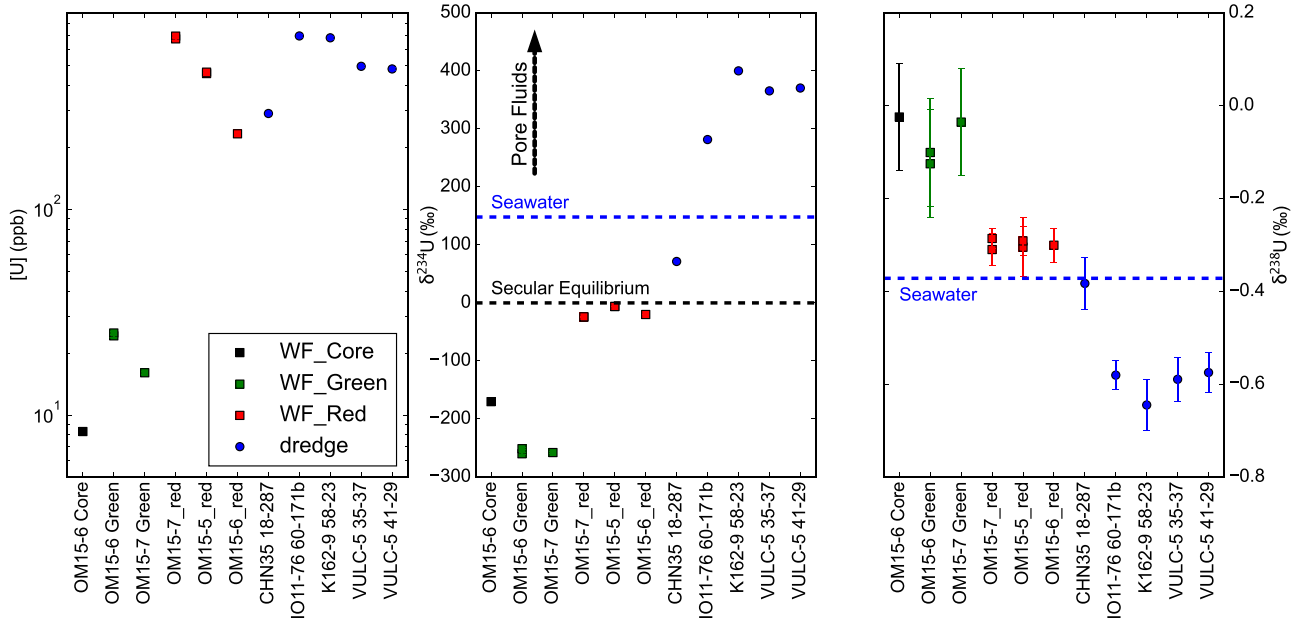

Fig. 2. U concentrations in ng/g (left panel), δ^{234}U values (center panel), and δ^{238}U values (right panel) for the samples discussed in this paper. Error bars are smaller than symbol sizes for U concentrations and δ^{234}U. Squares represent samples from Wadi Fins, with colors showing the respective weathering zones (core/black, green, and red). Seafloor serpentinites are shown as blue circles. Dashed black line in the left panel shows the secular equilibrium δ^{234}U = 0 ‰ value, the dashed blue line in the left panel shows the seawater δ^{234}U = 146.8 ‰ value, and the dashed blue line in the center panel shows the seawater δ^{238}U value of −0.379 ‰. The arrow pointing up in the center panel indicates the direction of high δ^{234}U values for sedimentary pore fluids (e.g. Henderson et al., 1999).

suggested that both serpentinization and weathering can be sources of this U addition (Kodolányi et al., 2011).

Our $\delta^{234}U$ results suggest that unaltered seawater cannot be the sole fluid source for U enrichment during seafloor weathering and/or serpentinization. Four of the five oceanic serpentinite samples have $\delta^{234}U$ values significantly higher than seawater, suggesting that these serpentinites incorporated U from $\delta^{234}U$ enriched fluids with $\delta^{234}U$ >145‰. Three possible fluid sources which will be evaluated in detail below are high-temperature hydrothermal fluids, low-temperature hydrothermal fluids, or sedimentary pore fluids. There are limited measurements of $\delta^{234}U$ in high-temperature vent fluids. Thus far none have been found to be above 200‰ (Chen et al., 1986), which are lower than our uppermost values of nearly 400‰. The $\delta^{234}U$ system is subject to resetting by radioactive production and decay. The ^{234}U half-life is 245, 620 years (Cheng et al., 2013), so in a closed system with no other processes causing continuous $\delta^{234}U$ deviations, $\delta^{234}U$ values will be reset to secular equilibrium ($\delta^{234}U = 0$) over five ^{234}U half-lives, or about 1.5 million years. The basement ages older than 1.5 Ma at all sites suggest that these samples should not have been exposed to high-temperature vent fluids recently enough to affect $\delta^{234}U$. Thus, we posit that high-temperature vent fluids are an unlikely source for the high $\delta^{234}U$ in these dredged serpentinites.

Instead we argue that U uptake into these dredged serpentinites must have happened during weathering processes occurring post-serpentinization, with a source from fluids that are chemically evolved from seawater. One potential fluid source is sedimentary pore fluids, which have high $\delta^{234}U$ due to alpha recoil ejection of ^{234}U from sediments to pore waters (Henderson et al., 1999; Ku et al., 1977; Maher et al., 2004). Another fluid source could be low-temperature fluids circulating through the ocean crust and shallow mantle. These fluids can be enriched in U (Mills and Dunk, 2010) and ferromanganese precipitates from low-temperature hydrothermal systems can have $\delta^{234}U$ values of up to 225 ‰ (Reyss et al., 1987). Uptake of U into serpentinites during weathering by ^{234}U-enriched low-temperature hydrothermal fluids is consistent with measured $\delta^{234}U$ at or near seawater values in altered but unweathered basalt (Bacon, 1978; MacDougall et al., 1979). Therefore while seawater may serve as an initial fluid source to serpentinite, the highly enriched $\delta^{234}U$ signals we observe requires subsequent overprinting of the original fluid signature.

The composition of the fluid source can be further investigated using U/Th, Rb/Th, and Cs/Th ratios. Rubidium and cesium are fluid-mobile but are not redox sensitive. Instead, Rb and Cs are highly sensitive to the formation of clay minerals, which strip them from solution (Spivack and Edmond, 1987). Most MOR serpentinites including the dredged samples in our study have U/Cs and U/Rb addition ratios higher than those of seawater by factors of ten and one hundred, respectively (Fig. 3). To our knowledge, combined measurements of Rb, Cs, and U have not been made on sedimentary pore fluids. However, sparse measurements from differing locations have shown sedimentary pore fluids to have U concentrations similar to or slightly lower than seawater (Santschi et al., 1988) and Rb and Cs concentrations higher than in seawater within upper sedimentary layers (James and Palmer, 2000). Thus, sedimentary pore fluids would have lower U/Cs and U/Rb ratios than seawater, the opposite direction of what we observe in serpentinites. Low-temperature crustal fluids from reducing environments experience significant U removal, minor Rb depletion, and Cs enrichment (Wheat et al., 2010), while colder crustal fluids from oxic environments have Rb and Cs similar to seawater and only 10% U depletion (Meyer et al., 2016). Composite altered ocean crust (AOC) samples have U/Cs ratios of 0.3 to 10.3 and U/Rb ratios of 0.004 to 0.13, with higher U/FME ratios generally found in deeper samples (Staudigel et al., 1996). These ratios are lower than the U/Cs and U/Rb addition ratios found for mid-ocean ridge serpentinites in Peters et al. (2017) and in the samples analyzed in this study. The Rb and Cs data are linearly correlated ($R^2 = 0.95$) in the AOC samples of Staudigel et al. (1996), but not correlated with U ($R^2 = 0.007$ for U and Cs, $R^2 = 0.03$ for U and Rb). This suggests Cs and Rb are taken up from fluids together, but independently of U during fluid flow through the ocean crust. We argue that the fluids contributing high $^{234}U/^{238}U$ to serpentinites have likely circulated through the upper ocean crust, progressively losing FME while exchanging U between the fluid and solid-phase. The fluids weathering the serpentinites in our study must be more evolved than even the fluids

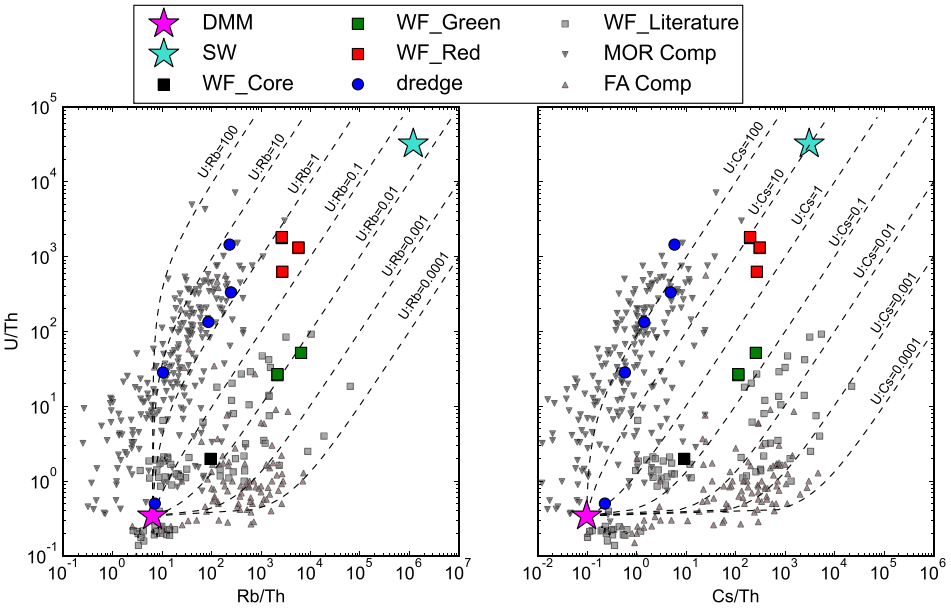

Fig. 3. Comparisons of U/Th with Rb/Th (left panel) and Cs/Th (right panel). Samples analyzed in this study are shown as large colored circles and squares, where abyssal serpentinites are blue circles, the Wadi Fins core zone is a black square, Wadi Fins green zones are green squares, and Wadi Fins red zones are red squares. The depleted mantle (Salters and Stracke, 2004) is shown as a large magenta star, and seawater (Chen et al., 1986; Li, 1991) is shown as a large blue star. Compilations of mid-ocean ridge serpentinites and forearc serpentinites (Peters et al., 2017) are shown as small downward-facing triangles and upward-facing triangles, respectively. Previous measurements of Samail Ophiolite serpentinites (Godard et al., 2021; Hanghøj et al., 2010) are shown as small gray squares. Dashed lines show addition lines starting from depleted mantle values for different U:Rb and U:Cs ratios.

weathering the upper ocean crust samples analyzed in Staudigel et al. (1996), as they have U/Cs and U/Rb addition ratios higher than those measured in the AOC.

The $\delta^{238}U$ values of most dredged serpentinites are also offset from seawater. Sample CHN35 18–287, the least altered sample in our suite, which has U/Th, Rb/Th, and Cs/Th similar to depleted mantle values (Fig. 4) is within error of modern seawater $\delta^{238}U$, but all other samples have $\delta^{238}U$ lower than seawater by up to 0.265 ‰. CHN 35 18–27 also has the lowest $\delta^{234}U$ values in our sample suite, roughly halfway between secular equilibrium and seawater. This value indicates that secondary alteration is responsible for both FME and U uptake in seafloor serpentinites.

Stable isotopic fractionation of U occurs during U isotope exchange between reduced and oxidized U and makes the reduced U(IV) in the solid phase isotopically heavy relative to soluble oxidized U(VI) (Weyer et al., 2008). Serpentinization typically occurs under highly reducing conditions, with oxygen fugacities sufficiently low to allow for microbial sulfate reduction (Alt and Shanks, 1998). However, incorporation of U in serpentinites by reductive addition during serpentinization from a seawater-like fluid should result in higher $\delta^{238}U$ in the serpentinite and is inconsistent with the $\delta^{238}U$ values similar to or lower than seawater measured in our samples.

Addition of U into oceanic serpentinites by fluids that have circulated through the ocean crust that results in $\delta^{234}U$ enrichment can also drive the $\delta^{238}U$ depletion we observe. Partial uranium reduction during fluid flow deposits solid-phase U with elevated $\delta^{238}U$ leaving the residual fluid with a lighter U isotope composition, for even a small amount of U reduction (Lau et al., 2020). A modest degree (<10% initial U removed) of U reduction during pore fluid flow is sufficient to generate fluids with 0.2–0.3 $\delta^{238}U$ depletion (Lau et al., 2020). Indeed, AOC samples analyzed by Andersen et al. (2015) had higher $\delta^{238}U$ values than either the bulk mantle or seawater (composite $\delta^{238}U = -0.170$ ‰). These high solid-phase values would isotopically complement the low $\delta^{238}U$ found in the seafloor serpentinites analyzed in this study. As these fluids weather serpentinites, the depleted $\delta^{238}U$ signal is imparted onto the solids.

We propose that these $\delta^{234}U$-enriched and $\delta^{238}U$-depleted fluids further alter already-serpentinized mantle rocks. All dredged samples are associated with seafloor topography from faulting and fracturing and may be affected by landslides and sedimentation, however dredging is usually performed on steep slopes with limited sediment. The fluids can chemically evolve through lateral flow and interaction with the igneous basement. After undergoing weathering, either these rocks were not exposed to pure seawater in the past 1.5 Ma or if they were exposed to seawater, then seawater alteration must have effectively ceased to prevent resetting serpentinite $\delta^{234}U$ to the seawater value of 145‰. The serpentinites may also be continuously weathered by a $\delta^{234}U$-enriched, $\delta^{238}U$-depleted fluid. Our suggestion of U uptake during weathering is corroborated by the rough correlation between U isotopes and the and the extent of alteration, as well as the correlation between $\delta^{234}U$ and $\delta^{238}U$ (Fig. 4). Sample CHN35 18–287, which has a $\delta^{234}U$ value of +71 ‰ that is intermediate between seawater and secular equilibrium and has a $\delta^{238}U$ value within error of seawater, is a partially serpentinized peridotite mylonite. The next lowest $\delta^{234}U$ value (+281 ‰) is from the core of a completely serpentinized peridotite after the outer weathered rind was removed. The remaining three samples are all moderately to pervasively weathered and have $\delta^{234}U$ values of more than 300 ‰ and $\delta^{238}U$ values less than −0.57 ‰.

Despite variations in degree of weathering, all samples show evidence of interaction with a $\delta^{234}U$-enriched, $\delta^{238}U$-depleted fluid in the past 1–1.5 My. The seafloor serpentinites analyzed in this study have $\delta^{234}U$ and $\delta^{238}U$ values that are correlated with both each other and with U concentrations (Fig. 4), despite being sampled from different ridge systems. The linear correlation between U isotopes and 1/[U] can be used to infer an isotopic composition of the fluid source through the y-intercept of a linear regression, assuming a single fluid source with a constant isotopic composition. We infer weathering fluid values of $\delta^{238}U = -0.799$ ‰ (linear regression $r^2 = 0.89$) and $\delta^{238}U = 587.3$ ‰ (linear regression $r^2 = 0.70$). Importantly, the observed correlation of both $\delta^{238}U$ and $\delta^{234}U$ with 1/[U] in serpentinites spanning these different ridge systems suggests the enrichment of $\delta^{234}U$ and depletion of $\delta^{238}U$ in evolved seawater within igneous basement rocks is a common phenomenon across the seafloor.

4.2. Processes controlling $\delta^{238}U$ at Wadi fins

The least altered core and green zone samples at Wadi Fins, consisting of partially to fully serpentinized peridotite, have relatively high $\delta^{238}U$ values of −0.125 to −0.025 ‰. The formation of the green zones is characterized by more extensive peridotite serpentinization and metasomatism (de Obeso and Kelemen, 2020). Green zones are enriched in U concentrations by a factor of 3 compared to cores in our samples, but this additional U is unfractionated in $\delta^{238}U$ at the 0.1‰ level (Fig. 2). Thus, it seems that in these samples, U addition associated with serpentinization comes from a source that is not isotopically distinct from the peridotite protolith, and that U uptake during this stage of serpentinization is non-fractionating.

There are limited measurements of $\delta^{238}U$ in igneous and metamorphic rocks (Li and Tissot, 2023), but the Wadi Fins core and green samples have higher $\delta^{238}U$ than almost all of them (Fig. 5). Andersen

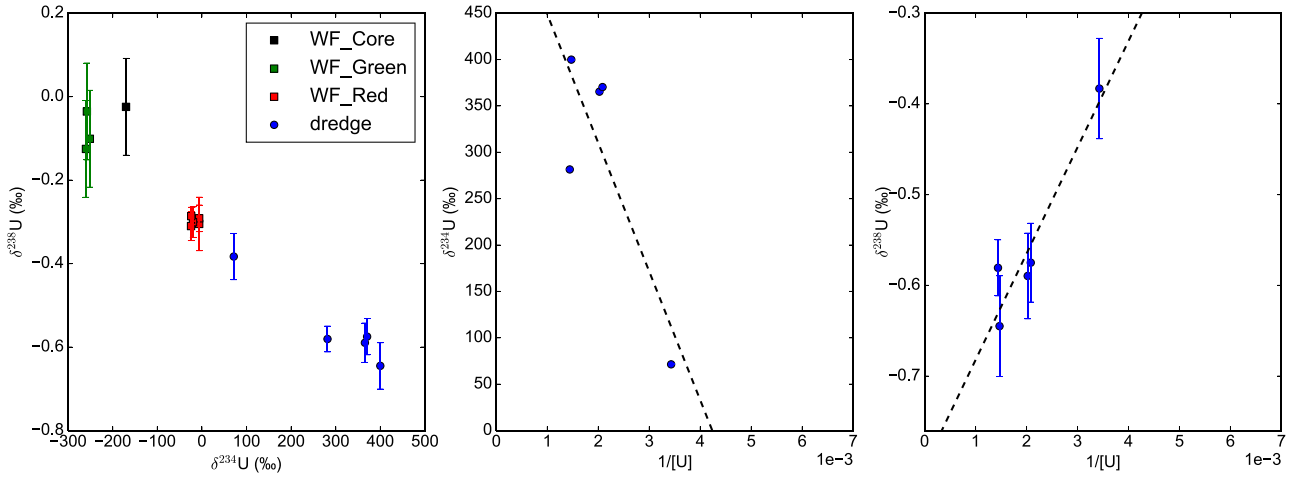

Fig. 4. Scatterplots showing relationships between $\delta^{238}U$ and $\delta^{234}U$ in all samples measured in this study, as well the relationships between $\delta^{234}U$ and $\delta^{238}U$ with 1/[U]. Solid lines show best-fit linear regressions for 1/U vs. $\delta^{234}U$ (center) and $\delta^{238}U$ (right).

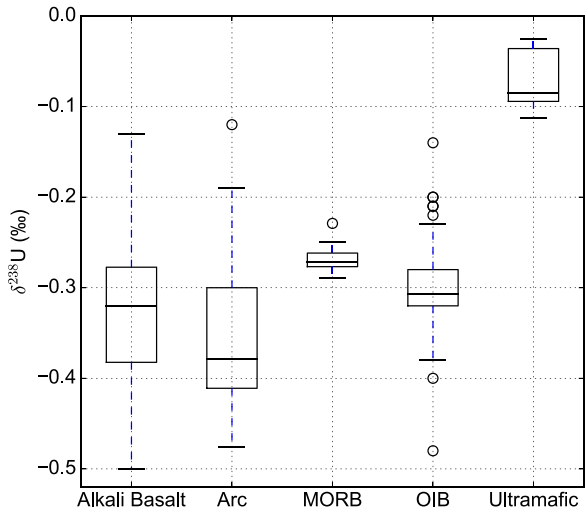

Fig. 5. Comparison of $\delta^{238}U$ measurements in different igneous rock types, compiled from the Uranium Isotope Database (Li and Tissot, 2023). Ultramafic rocks DTS-2b (Amelin et al., 2010; Iizuka et al., 2014) and Wadi Fins core and green (this study) grouped into the right box have higher $\delta^{238}U$ than nearly all previously measured igneous rocks, including alkali basalts (Stirling et al., 2005), mid-ocean ridge basalts (Andersen et al., 2015; Stirling et al., 2005), ocean island basalts (Andersen et al., 2015; Gaschnig et al., 2021a, 2021b), and arc lavas (Andersen et al., 2015; Avanzinelli et al., 2018; Freymuth et al., 2019).

et al. (2015) found that mid-ocean ridge basalts (MORBs) have $\delta^{238}U$ of -0.268 ± 0.011 ‰, ocean island basalts (OIBs) have $\delta^{238}U$ of -0.308 ± 0.005 ‰, and volcanic rocks from the Mariana arc have $\delta^{238}U$ as light as -0.419 ‰. Other measurements of arc volcanics found heavier $\delta^{238}U$ of -0.2 to -0.1 ‰ in sediment-dominated melts from Mt. Vesuvius (Avanzinelli et al., 2018) and $\delta^{238}U$ lighter than MORB at the Izu arc (Freymuth et al., 2019). Other measurements of OIBs have found $\delta^{238}U$ between -0.4 and -0.2 ‰ with no apparent impact of magmatic differentiation on $\delta^{238}U$ (Gaschnig et al., 2021a, 2021b). While $\delta^{238}U$ in Wadi Fins core and green zones is higher than all these previously measured igneous rocks, it is similar to the DTS-2b dunite USGS geostandard which has two $\delta^{238}U$ measurements of -0.085 ± 0.085 ‰ and -0.094 ± 0.094 ‰ (Amelin et al., 2010; Iizuka et al., 2014). The DTS-2b standard is sourced from the Twin Sisters Mountain, an ultramafic dunite with very low degrees of background serpentinization, increasing in discrete fault zones (Ragan, 1963). While Wadi Fins core and green samples are primarily harzburgites (de Obeso and Kelemen, 2020) and share an ultramafic lithology with DTS-2b, the Wadi Fins samples are more serpentinized. Albeit a limited dataset, the high $\delta^{238}U$ values of DTS-2b and Wadi Fins ultramafic samples compared to all other igneous rocks could represent a significantly different $\delta^{238}U$ of mantle peridotite than has previously been inferred and warrants additional study. Another possibility is that reductive addition of U during serpentinization imparts high $\delta^{238}U$ values onto the Wadi Fins core and green zones. These zones both have U/Th, Rb/Th, and Cs/Th elevated above depleted mantle ratios, indicating U and FME uptake during serpentinization (Fig. 3). However, the core and green zones have much different degrees of serpentinization as indicated by the factor of 2 higher loss on ignition in green zones (Table S1, de Obeso and Kelemen, 2020), and both are more serpentinized than the ultramafic dunite of the Twin Sisters Mountain source of DTS-2b. These observations would suggest that U uptake during serpentinization is not fractionating or contributes reduced, high-$\delta^{238}U$ to protolith rocks, and that the high $\delta^{238}U$ of ultramafic rocks is more likely due to different initial $\delta^{238}U$ for mantle peridotite than previously documented.

While $\delta^{238}U$ values do not change within analytical uncertainty from core to green zones, they are significantly lower in red zones, averaging -0.298 ± 0.020 ($n = 5$, 2-sigma standard deviation). The red zone of the Wadi Fins serpentinite is characterized by iron oxides and cross-cutting carbonate veins, with goethite grown within the serpentinite and magnetite appearing in the carbonate veins (Cooperdock et al., 2020; de Obeso and Kelemen, 2020). When analyzing the red zone samples, we were careful to avoid sampling carbonate veins while preparing rock powders. Carbonate contents measured on Wadi Fins powders do not correlate with U isotopic compositions for either $\delta^{234}U$ or $\delta^{238}U$ across weathering zones (Fig. 6). Thus, the factor of 50 enrichment we observe in U concentrations within red zones compared to the green zones is associated with the rock itself and not due to the presence of high-U carbonate in our samples.

We argue that U uptake in red zone samples occurs due to coprecipitation with Fe oxides and oxyhydroxides, based on U/FME ratios (Fig. 3). Core and green samples plot along U/Rb and U/Cs addition ratio isolines of 0.01 and 0.2, respectively (Fig. 3). This is consistent with FME addition ratio values previously reported for other Samail Ophiolite samples (gray squares in Fig. 3) (Godard et al., 2021; Hanghøj et al., 2010). However, red zones are significantly more enriched in U compared to Rb and Cs, plotting along U/Rb and U/Cs addition ratio lines an order of magnitude higher than the rest of the Wadi Fins samples. While iron oxides have a strong affinity for U uptake (Duff et al., 2002), there seems to be little association of alkali elements like Rb and Cs with iron oxides (Li, 1982; Musić and Ristić, 1988). Thus the U enrichment in red zones compared to green zones occurs with no associated Rb or Cs enrichment.

We hypothesize that U coprecipitated with Fe oxides and Fe-oxyhydroxides in the red zones may be originally sourced from fluids that weathered the limestone sediments overlying Wadi Fins (Fig. 7). This fluid pathway is consistent with petrology and modeling results of de Obeso and Kelemen (2020). The isotopic balance supporting this argument is as follows. Limestone sediments overlying Wadi Fins were deposited starting in the late Cretaceous/Early Paleocene (Schlüter et al., 2008). Since measurements of ferromanganese crust $\delta^{238}U$ suggest no secular trend in seawater $\delta^{238}U$ from 80 Ma to present (Wang et al., 2016), the overlying limestones likely precipitated from seawater with $\delta^{238}U$ similar to today's value of -0.379 ‰ (Kipp et al., 2022). Because carbonate sediments in modern shallow carbonate environments have higher $\delta^{238}U$ than seawater by 0.24–0.28 ‰ (Chen et al., 2018; Tissot et al., 2018) we expect the overlying limestones to have $\delta^{238}U$ higher than Cenozoic seawater by this 0.24–0.28 ‰ and have $\delta^{238}U$ values of -0.139 to -0.099 ‰. We argue that fluids would weather U of this isotopic composition from the limestones, then these alkaline, U-rich fluids then precipitate U alongside Fe oxides and Fe-oxyhydroxides in Wadi Fins red zones. Coprecipitation and/or adsorption onto Fe oxides results in solid-phase U that is -0.24 ‰ offset from solution (Goto et al., 2014), pushing our presumed red zone $\delta^{238}U$ to -0.379 to -0.339 ‰ - comparable, though slightly lower, than our average red zone $\delta^{238}U$ of -0.298 ‰ (Fig. 7). A small additional contribution of U from oxidative weathering of reduced, isotopically heavy U(IV) from the overlying limestone sediments, would be sufficient to make up this difference. Because this additional U is added in association with Fe oxides, its isotopic signature is only found in the red zones, where the Fe oxides are present. Critically, our interpretation argues that the $\delta^{238}U$ of the red zone in the studied serpentinite from Wadi Fins was set primarily by processes happening before 1.5 Ma, allowing the $\delta^{234}U$ in red zones to reach secular equilibrium again.

4.3. Mineralogical controls on $\delta^{234}U$ at Wadi fins

At the Wadi Fins site, samples from the core, green, and red zones display a remarkable 240‰ $\delta^{234}U$ variation over 30 cm spatial scales (Fig. 1). The serpentinite samples at Wadi Fins analyzed in this study experienced fluid-rock interactions and calcite veining that resulted in the bulk chemical and mineral core-green-red zonation at minimum 15 Ma, and possibly 60 Ma (Cooperdock et al., 2020; de Obeso and Kelemen, 2020, 2018). Importantly, this indicates that the background U and

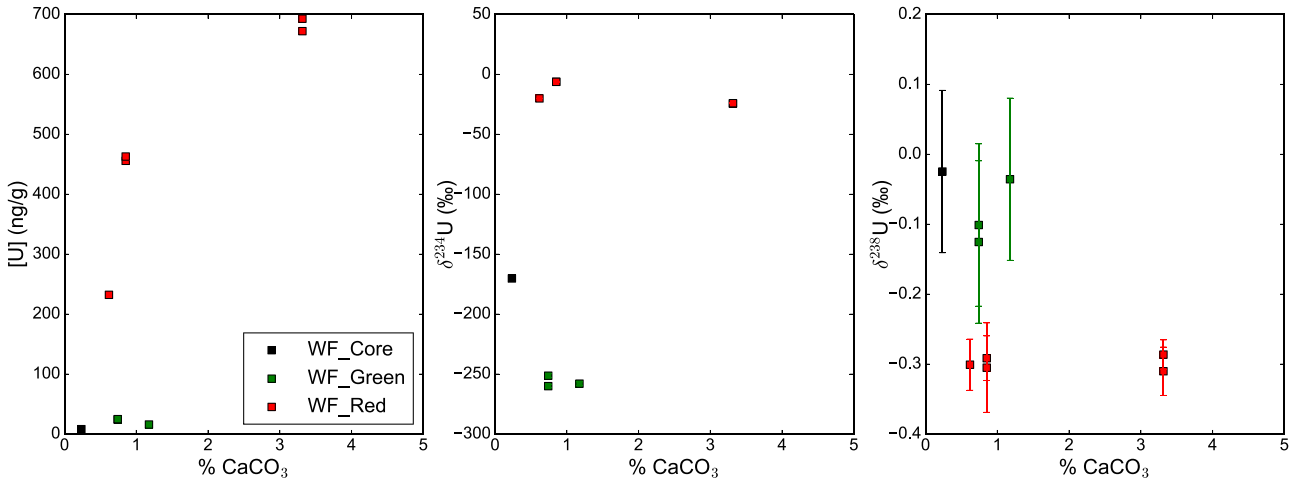

Fig. 6. Scatterplots relating measured calcium carbonate content with [U], $\delta^{234}U$, and $\delta^{238}U$ for Wadi Fins rocks. No distinct relationship is observed between calcium carbonate content and uranium isotopic composition either within or across alteration zones. Error bars are smaller than symbol sizes for [U] and $\delta^{234}U$.

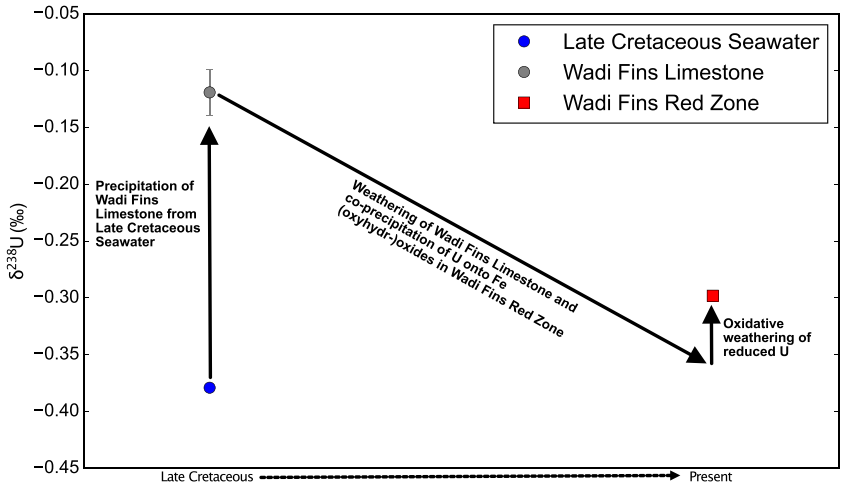

Fig. 7. Schematic showing processes resulting in measured $\delta^{238}U$ of Wadi Fins red zones. Limestone overlying Wadi Fins precipitated from Late Cretaceous Seawater with relatively heavy $\delta^{238}U$. As meteoric waters weather the limestone, they mobilize U and flow through the Wadi Fins serpentinite, where U is co-precipitated on Fe-oxides/oxyhydroxides. Some degree of oxidative weathering of reduced U within the overlying limestone is necessary for this sequence of events to result in the measured red zone $\delta^{238}U$.

Fe(III) concentration patterns in the zoned serpentinite likely reflect processes that occurred long before the 1.5 Myr timescale recorded by $\delta^{234}U$. We thus interpret the negative $\delta^{234}U$ values as evidence for either recent or steady state processes acting on the uranium in the Wadi Fins serpentinites.

Aqueous weathering tends to lower solid-phase $\delta^{234}U$ while enriching fluid $\delta^{234}U$. Two processes give rise to $\delta^{234}U$ fractionation during aqueous weathering. First, preferential leaching of ^{234}U relative to ^{238}U can occur during water rock interaction, since the energy from alpha decay of ^{238}U decaying to ^{234}Th will damage the mineral lattice site hosting its decay product ^{234}U (Andersen et al., 2009; Fleischer, 1980). Second, the ^{234}Th nuclide can be directly ejected from the mineral lattice following ^{238}U decay (DePaolo et al., 2012, 2006).

Preferential leaching of ^{234}U as the process driving $\delta^{234}U$ at Wadi Fins would require a way for greater ^{234}U leaching to occur in the core and green zones. The Wadi Fins samples analyzed in this study were collected from the floor of a canyon, where core, green, and red zones are all exposed at the surface of the canyon floor. Given the petrologic and geochemical evidence that serpentinization and chemical zonation in the Wadi Fins rocks analyzed here occurred tens of millions of years ago, and that the weathering zones are within 30 cm of each other, it is likely that the core, green, and red zones analyzed in this study experienced the same degree of meteoric surface weathering over the last 1.5 My during episodic canyon flooding, both during dry periods and pluvials. Thus, we argue that it is unlikely for preferential leaching of ^{234}U to be much greater in core and green zones than in red zones. Instead, we make the argument that the variable $\delta^{234}U$ depletions we observe are likely due to direct ejection.

The magnitude of the solid-phase $\delta^{234}U$ depletion due to direct ejection depends on the size and geometry of the mineral grains hosting U (DePaolo et al., 2012, 2006). Smaller grains, and grains with higher surface area to volume ratios, will lose more ^{234}Th (and thus ^{234}U) by direct ejection from the grain compared to larger, rounder grains (DePaolo et al., 2006; Kigoshi, 1971). The fraction of ^{238}U decay products that escape the grain (f_α) is a function of the recoil distance L (we follow Maher et al. (2006) in using a recoil length of 30 nm for silicate minerals), grain diameter d, and a parameter λ_r that accounts for the effects of both surface roughness and grain shape differences from a perfect sphere, where larger λ_r values represent greater surface roughness and more oblate shapes (Kigoshi, 1971; Lee et al., 2010; Maher et al., 2006):

1) $f_\alpha = \frac{3L}{2d} * \lambda_r$

Previous studies determining f_α have been done on sedimentary rocks of known or measured grain size, with the aim of dating their comminution (Aciego et al., 2011; DePaolo et al., 2012, 2006; Lee et al., 2010; Maher et al., 2006, 2004). Given the shared geologic history over the last 1.5 Myr, we interpret the measured $^{234}U/^{238}U$ depletions at Wadi Fins in terms of grain size and/or shape differences in the minerals hosting U between the core, green, and red weathering zones. We can use the measured $\delta^{234}U$ depletions, converted to f_α, to calculate the grain size of the minerals likely hosting U in the samples. We note that this calculation only is for the grain sizes of the primary mineral hosts of U, not for the grain size of the whole rock.

Fig. 8 graphically shows the range of grain sizes possible for the minerals hosting U in the Wadi Fins weathering zones based on $\delta^{234}U$. The boxes span λ_r values from 1 to 15. Our calculations show that core and green zone samples have grains hosting U that can range from approximately 0.2 to 5 μm, while red zone samples have U hosting grain sizes of about 2–70 μm. We do not have direct constraints on λ_r for these samples. However, electron microprobe analyses with a spot size of 10 μm performed by de Obeso and Kelemen (2020) found no pure goethite. Thus, the iron oxide grains we argue host U in the red zones must be smaller than 10 μm, narrowing our range of possible scenarios (black and blue ellipses in Fig. 8). If grain size differences in the minerals hosting U between core, green, and red zones solely drive the $\delta^{234}U$ depletions in these zones, then U host minerals must have 0.2–0.3 μm diameters in core and green zones, and 4–5 μm diameters in red zones (black ellipse in Fig. 8). Alternatively, if grain shape differences between U mineral hosts in core, green, and red zones solely drive the $\delta^{234}U$ depletions in these zones, then U would be hosted in grains 2–3 μm in diameter in all zones, with λ_r values of 10–15 in core and green zones and 1 in red zones, suggesting that U hosting minerals in core and green zones are highly oblate and/or rough, and U hosting minerals in red zones are highly spherical and/or smooth (blue ellipse in Fig. 8). Of course, a range of possibilities exist between the grain size and grain shape hypothesis endmembers, where slightly smaller and slightly more oblate minerals host U in core and green zones, and slightly larger (but <5 μm) and slightly more spherical minerals host U in red zones. These possibilities lead us to speculatively propose that U is hosted in fine-grained, sheet silicates in core and green zones, and dominantly in somewhat coarser, more spherical iron oxides in red zones.

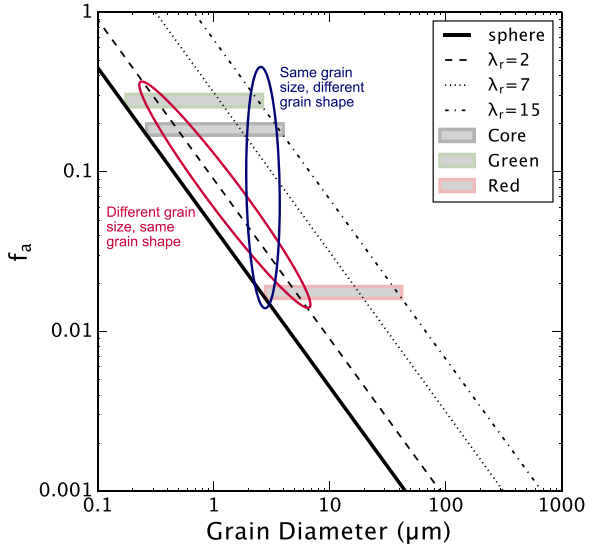

Fig. 8. Measured fractional ^{234}U removal (f_α) for Wadi Fins core, green, and red zones, and associated grain diameter predicted by equation 1. The sample boxes span a range of surface roughness values (λ_r) from 1 (sphere) to 15 – the f_α-grain diameter relationships are shown as solid or dashed lines for different λ_r values. Red zone samples with substantially less preferential ^{234}U removal than green and core zone samples, suggesting that U in red zones is hosted in minerals with larger grain sizes and/or more spherical shapes. The black ellipse outlines the range of possible grain sizes and shapes for a situation where grain size alone dictates the $\delta^{234}U$ differences between core, green, and red zones, and the blue ellipse outlines the range of grain sizes and shapes if grain shape alone controls $\delta^{234}U$ differences between core, green, and red zones.

5. Conclusions and implications

The uranium isotope signatures we have measured in oceanic and continental serpentinites are significantly different from typical volcanic rocks and seawater, suggesting that post-formation weathering, both submarine and subaerial, exerts a strong control on the dynamics of U and possibly other fluid-mobile elements. We posit that serpentinites primarily take up uranium during oxidative weathering, while serpentinization alone adds little uranium. Thus the uranium isotopic composition of serpentinites reflects the isotopic composition of the late-stage weathering fluids that overprint the original U isotopic compositions. The enrichment of U and $\delta^{234}U$ in oceanic serpentinites shows that weathering of these serpentinites must have occurred <1.5 Ma, by reaction with evolved fluids that have circulated through the oceanic crust. We argue that this signature reflects U uptake during weathering after serpentinization. This alteration process must cease before the serpentinites are exhumed and exposed to seawater at the seafloor or be ongoing, otherwise their $\delta^{234}U$ value would reset to the seawater value.

We propose that the >250 ‰ range in $\delta^{234}U$ values across 30 cm spatial scales at Wadi Fins is likely the result of varying grain size and/or shape of minerals hosting U in different weathering zones. If correct, this means that physicochemical properties of minerals are critical for setting the U content of serpentinite, a hypothesis that could be tested in future work since the specific mineral(s) hosting U in serpentinite are currently unknown.

One of the original goals of this study was to investigate whether the $\delta^{238}U$ of serpentinites faithfully recorded the $\delta^{238}U$ of seawater. Our finding that $\delta^{238}U$ is offset from seawater in both submarine and subaerial serpentinites suggests that weathering reactions with both meteoric and oceanic waters result in offsets between serpentinite and seawater $\delta^{238}U$. In seafloor settings, this is due to uptake of U from evolved fluids that are isotopically fractionated from seawater. At Wadi Fins, we suggest this could be due to secondary deposition of U coprecipitating with iron oxides on serpentinite surfaces. The data in this study suggests serpentinite U uptake from evolved fluids is a pervasive phenomenon across multiple seafloor settings, and must be taken into account when determining paleo seawater $\delta^{238}U$ compositions from serpentinites.

While our sample set is admittedly limited, we see evidence for systematic submarine and subaerial weathering processes in setting the uranium isotopic composition of serpentinites. Taken together, our results align well with the recent study of Geilert et al. (2020) in diagnosing the critical importance of post-serpentinization weathering reactions. Further work investigating the fluids and processes delivering different elements to serpentinites will be critical for assessing the validity of ancient seawater chemistry reconstructions from serpentinite, as well as for determining the composition of fluid-mobile elements and gasses carried to the mantle by subduction of oceanic serpentinite. We hope that this initial study paves the way for additional investigation of peridotite and serpentinite fluid uptake, weathering, and formation conditions using uranium isotopes.

CRediT authorship contribution statement

Frank J. Pavia: Methodology, Formal analysis, Investigation, Conceptualization, Writing – original draft, Writing – review & editing. **Emily H.G. Cooperdock:** Writing – original draft, Writing – review & editing, Conceptualization, Resources. **Juan Carlos de Obeso:** Writing –

original draft, Writing – review & editing, Conceptualization, Resources. **Kenneth W.W. Sims:** Writing – review & editing. **François L.H. Tissot:** Resources, Writing – review & editing. **Frieder Klein:** Resources, Writing – review & editing.

Declaration of Competing Interest

The authors declare that they have no known competing financial interests or personal relationships that could have appeared to influence the work reported in this paper.

Data availability

All data is included within the tables in the paper and supplement.

Acknowledgements

F.J.P. was supported by a Stanback Postdoctoral Fellowship at Caltech. EHGC was supported by U.S. National Science Foundation (NSF) grants EAR-1949148 and OCE-2049940 and start-up funds from USC. FLHT is grateful for support from NSF grants EAR-1824002 and MGG-2054892, a Packard Fellowship, a research award from the Heritage Medical Research Institute, and start-up funds provided by Caltech. F.K. was supported by the Independent Research & Development Program "Chemical Weathering of the Oceanic Mantle by Seawater" at WHOI. KWWS acknowledges support from NSF-OCE-1634669. We thank Will Berelson and Nick Rollins at University of Southern California for facilitating the carbonate content measurements. The comments of two anonymous reviewers, as well as the associate editor Laurence Coogan, greatly improved the manuscript.

Supplementary materials

Supplementary material associated with this article can be found, in the online version, at doi:10.1016/j.epsl.2023.118434.

References

Aciego, S., Bourdon, B., Schwander, J., Baur, H., Forieri, A., 2011. Toward a radiometric ice clock: uranium ages of the Dome C ice core. Quaternary Sci. Rev. 30, 2389–2397. https://doi.org/10.1016/j.quascirev.2011.06.008.

Alt, J.C., Shanks, W.C., 1998. Sulfur in serpentinized oceanic peridotites: serpentinization processes and microbial sulfate reduction. J. Geophys. Res. Solid Earth 103, 9917–9929. https://doi.org/10.1029/98jb00576.

Amelin, Y., Kaltenbach, A., Iizuka, T., Stirling, C.H., Ireland, T.R., Petaev, M., Jacobsen, S.B., 2010. U–Pb chronology of the Solar System's oldest solids with variable 238U/235U. Earth Planet Sc. Lett. 300, 343–350. https://doi.org/10.1016/j.epsl.2010.10.015.

Andersen, M.B., Elliott, T., Freymuth, H., Sims, K.W.W., Niu, Y., Kelley, K.A., 2015. The terrestrial uranium isotope cycle. Nature 517, 356–U463. https://doi.org/10.1038/nature14062.

Andersen, M.B., Erel, Y., Bourdon, B., 2009. Experimental evidence for ^{234}U–^{238}U fractionation during granite weathering with implications for $^{234}U/^{238}U$ in natural waters. Geochim Cosmochim Ac 73, 4124–4141. https://doi.org/10.1016/j.gca.2009.04.020.

Andersen, M.B., Stirling, C.H., Weyer, S., 2017. Uranium isotope fractionation. Revi. Mineral. Geochem. 82, 799–850. https://doi.org/10.2138/rmg.2017.82.19.

Avanzinelli, R., Casalini, M., Elliott, T., Conticelli, S., 2018. Carbon fluxes from subducted carbonates revealed by uranium excess at Mount Vesuvius, Italy. Geology 46, 259–262. https://doi.org/10.1130/g39766.1.

Bacon, M.P., 1978. Radioactive disequilibrium in altered mid-oceanic basalts. Earth Planet Sc Lett. 39, 250–254. https://doi.org/10.1016/0012-821x(78)90200-5.

Beinlich, A., Austrheim, H., Mavromatis, V., Grguric, B., Putnis, C.V., Putnis, A., 2018. Peridotite weathering is the missing ingredient of Earth's continental crust composition. Nat. Commun. 9, 634. https://doi.org/10.1038/s41467-018-03039-9.

Chen, J.H., Edwards, R.L., Wasserburg, G.J., 1986. ^{238}U, ^{234}U and ^{232}Th in seawater. Earth Planet. Sci. Lett. 80, 241–251. https://doi.org/10.1016/0012-821x(86)90108-1.

Chen, X., Romaniello, S.J., Herrmann, A.D., Hardisty, D., Gill, B.C., Anbar, A.D., 2018. Diagenetic effects on uranium isotope fractionation in carbonate sediments from the Bahamas. Geochim Cosmochim Ac 237, 294–311. https://doi.org/10.1016/j.gca.2018.06.026.

Cheng, H., Edwards, R.L., Shen, C.C., Polyak, V.J., Asmerom, Y., Woodhead, J., Hellstrom, J., Wang, Y., Kong, X., Spötl, C., Wang Jr., X., 2013. Improvements in ^{230}Th dating, ^{230}Th and ^{234}U half-life values, and U–Th isotopic measurements by multi-collector inductively coupled plasma mass spectrometry. Earth Planet. Sci. Lett. 371–372, 82–91. https://doi.org/10.1016/j.epsl.2013.04.006.

Cooperdock, E.H.G., Stockli, D.F., Kelemen, P.B., Obeso, J.C., 2020. Timing of magnetite growth associated with peridotite-hosted carbonate veins in the SE Samail Ophiolite, Wadi Fins, Oman. J. Geophys. Res. Solid Earth 125. https://doi.org/10.1029/2019jb018632.

D'Andres, J., Kendrick, M.A., Bennett, V.C., Nutman, A.P., 2019. Halogens in serpentinites from the Isua supracrustal belt, Greenland: an Eoarchean seawater signature and biomass proxy? Geochim Cosmochim Ac 262, 31–59. https://doi.org/10.1016/j.gca.2019.07.017.

de Obeso, J.C., Kelemen, P.B., 2018. Fluid rock interactions on residual mantle peridotites overlain by shallow oceanic limestones: insights from Wadi Fins, Sultanate of Oman. Chem. Geol. 498, 139–149. https://doi.org/10.1016/j.chemgeo.2018.09.022.

de Obeso, J.C., Kelemen, P.B., 2020. Major element mobility during serpentinization, oxidation and weathering of mantle peridotite at low temperatures. Philos. Trans. R. Soc. A. https://doi.org/10.1098/rsta.2018.0433.

de Obeso, J.C., Ramos, D.P.S., Higgins, J.A., Kelemen, P.B., 2021. A Mg isotopic perspective on the mobility of magnesium during serpentinization and carbonation of the oman ophiolite. J. Geophys. Res. Solid Earth 126. https://doi.org/10.1029/2020jb020237.

DePaolo, D.J., Lee, V.E., Christensen, J.N., Maher, K., 2012. Uranium comminution ages: sediment transport and deposition time scales. C R Geosci. 344, 678–687. https://doi.org/10.1016/j.crte.2012.10.014.

DePaolo, D.J., Maher, K., Christensen, J.N., McManus, J., 2006. Sediment transport time measured with U-series isotopes: results from ODP North Atlantic drift site 984. Earth Planet. Sci. Lett. 248, 394–410. https://doi.org/10.1016/j.epsl.2006.06.004.

Deschamps, F., Godard, M., Guillot, S., Hattori, K., 2013. Geochemistry of subduction zone serpentinites: a review. Lithos 178, 96–127. https://doi.org/10.1016/j.lithos.2013.05.019.

Dick, H.J.B., 1989. Abyssal peridotites, very slow spreading ridges and ocean ridge magmatism. Geological Soc. Lond. Special Publ. 42, 71–105. https://doi.org/10.1144/gsl.sp.1989.042.01.06.

Dong, S., Wang, X.T., Subhas, A.V., Pavia, F.J., Adkins, J.F., Berelson, W.M., 2022. Depth profiles of suspended carbon and nitrogen along a North Pacific transect: concentrations, isotopes, and ratios. Limnol. Oceanogr. 67, 247–260. https://doi.org/10.1002/lno.11989.

Duff, M.C., Coughlin, J.U., Hunter, D.B., 2002. Uranium co-precipitation with iron oxide minerals. Geochim Cosmochim Ac 66, 3533–3547. https://doi.org/10.1016/s0016-7037(02)00953-5.

Fleischer, R.L., 1980. Isotopic disequilibrium of uranium: alpha-recoil damage and preferential solution effects. Science 207, 979–981. https://doi.org/10.1126/science.207.4434.979.

Freymuth, H., Andersen, M.B., Elliott, T., 2019. Uranium isotope fractionation during slab dehydration beneath the Izu arc. Earth Planet. Sci. Lett. 522, 244–254. https://doi.org/10.1016/j.epsl.2019.07.006.

Gaschnig, R.M., Rader, S.T., Reinhard, C.T., Owens, J.D., Planavsky, N., Wang, X., Asael, D., Greaney, A., Helz, R., 2021a. Behavior of the Mo, Tl, and U isotope systems during differentiation in the Kilauea Iki lava lake. Chem. Geol. 574, 120239 https://doi.org/10.1016/j.chemgeo.2021.120239.

Gaschnig, R.M., Reinhard, C.T., Planavsky, N.J., Wang, X., Asael, D., Jackson, M.G., 2021b. The impact of primary processes and secondary alteration on the stable isotope composition of ocean island basalts. Chem. Geol. 581, 120416 https://doi.org/10.1016/j.chemgeo.2021.120416.

Geilert, S., Grasse, P., Wallmann, K., Liebetrau, V., Menzies, C.D., 2020. Serpentine alteration as source of high dissolved silicon and elevated $\delta^{30}Si$ values to the marine Si cycle. Nat. Commun. 11, 5123. https://doi.org/10.1038/s41467-020-18804-y.

Godard, M., Carter, E.J., Decrausaz, T., Lafay, R., Bennett, E., Kourim, F., Obeso, J.C., Michibayashi, K., Harris, M., Coggon, J.A., Teagle, D.A.H., Kelemen, P.B., Party, 2021. Geochemical profiles across the listvenite-metamorphic transition in the basal megathrust of the semail ophiolite: results from drilling at OmanDP Hole BT1B. J. Geophys. Res.: Solid Earth 126. https://doi.org/10.1029/2021jb022733.

Goto, K.T., Anbar, A.D., Gordon, G.W., Romaniello, S.J., Shimoda, G., Takaya, Y., Tokumaru, A., Nozaki, T., Suzuki, K., Machida, S., Hanyu, T., Usui, A., 2014. Uranium isotope systematics of ferromanganese crusts in the Pacific Ocean: implications for the marine $^{238}U/^{235}U$ isotope system. Geochim Cosmochim Ac 146, 43–58. https://doi.org/10.1016/j.gca.2014.10.003.

Hanghøj, K., Kelemen, P.B., Hassler, D., Godard, M., 2010. Composition and genesis of depleted mantle peridotites from the Wadi Tayin Massif, Oman Ophiolite; Major and Trace Element Geochemistry, and Os Isotope and PGE Systematics. J. Pet. 51, 201–227. https://doi.org/10.1093/petrology/egp077.

Henderson, G.M., Slowey, N.C., Haddad, G.A., 1999. Fluid flow through carbonate platforms: constraints from $^{234}U/^{238}U$ and Cl - in Bahamas pore-waters. Earth Planet. Sci. Lett. 169, 99–111. https://doi.org/10.1016/s0012-821x(99)00065-5.

Iizuka, T., Amelin, Y., Kaltenbach, A., Koefoed, P., Stirling, C.H., 2014. U–Pb systematics of the unique achondrite Ibitira: precise age determination and petrogenetic implications. Geochim Cosmochim Ac 132, 259–273. https://doi.org/10.1016/j.gca.2014.02.017.

James, R.H., Palmer, M.R., 2000. Marine geochemical cycles of the alkali elements and boron: the role of sediments. Geochim. Cosmochim. Acta 64, 3111–3122. https://doi.org/10.1016/s0016-7037(00)00418-x.

Kendrick, M.A., Scambelluri, M., Honda, M., Phillips, D., 2011. High abundances of noble gas and chlorine delivered to the mantle by serpentinite subduction. Nat. Geosci. 4, 807–812. https://doi.org/10.1038/ngeo1270.

Kigoshi, K., 1971. Alpha-Recoil thorium-234: dissolution into water and the uranium-234/uranium-238 disequilibrium in nature. Science 173, 47–48. https://doi.org/10.1126/science.173.3991.47.

Kipp, M.A., Li, H., Ellwood, M.J., John, S.G., Middag, R., Adkins, J.F., Tissot, F.L.H., 2022. ^{238}U, ^{235}U and ^{234}U in seawater and deep-sea corals: a high-precision reappraisal. Geochim Cosmochim Ac 336, 231–248. https://doi.org/10.1016/j.gca.2022.09.018.

Klein, F., Bach, W., Humphris, S.E., Kahl, W.A., Jöns, N., Moskowitz, B., Berquó, T.S., 2014. Magnetite in seafloor serpentinite—some like it hot. Geology 42, 135–138. https://doi.org/10.1130/g35068.1.

Klein, F., Bach, W., McCollom, T.M., 2013. Compositional controls on hydrogen generation during serpentinization of ultramafic rocks. Lithos 178, 55–69. https://doi.org/10.1016/j.lithos.2013.03.008.

Klein, F., Humphris, S.E., Bach, W., 2020. Brucite formation and dissolution in oceanic serpentinite. Geochem. Perspectives Lett. 1–5. https://doi.org/10.7185/geochemlet.2035.

Klein, F., Marschall, H.R., Bowring, S.A., Humphris, S.E., Horning, G., 2017. Mid-ocean ridge serpentinite in the Puerto Rico trench: from seafloor spreading to subduction. J. Petrol. 58, 1729–1754. https://doi.org/10.1093/petrology/egx071.

Kodolányi, J., Pettke, T., Spandler, C., Kamber, B.S., Gméling, K., 2011. Geochemistry of ocean floor and fore-arc serpentinites: constraints on the ultramafic input to subduction zones. J. Petrol. 53, 235–270. https://doi.org/10.1093/petrology/egr058.

Ku, T.L., Mathieu, G.G., Knauss, K.G., 1977. Uranium in open ocean: concentration and isotopic composition. Deep Sea Res. 24, 1005–1017. https://doi.org/10.1016/0146-6291(77)90571-9.

Lau, K.V., Lyons, T.W., Maher, K., 2020. Uranium reduction and isotopic fractionation in reducing sediments: insights from reactive transport modeling. Geochim Cosmochim Ac 287, 65–92. https://doi.org/10.1016/j.gca.2020.01.021.

Lee, V.E., DePaolo, D.J., Christensen, J.N., 2010. Uranium-series comminution ages of continental sediments: case study of a Pleistocene alluvial fan. Earth Planet Sc Lett. 296, 244–254. https://doi.org/10.1016/j.epsl.2010.05.005.

Li, H., Tissot, F.L.H., 2023. UID: the uranium isotope database. Chem. Geol. 618, 121221 https://doi.org/10.1016/j.chemgeo.2022.121221.

Li, Y.H., 1991. Distribution patterns of the elements in the ocean: a synthesis. Geochim. Cosmochim. Acta 55, 3223–3240. https://doi.org/10.1016/0016-7037(91)90485-n.

Li, Y.H., 1982. Interelement relationship in abyssal Pacific ferromanganese nodules and associated pelagic sediments. Geochim. Cosmochim. Acta 46, 1053–1060. https://doi.org/10.1016/0016-7037(82)90058-8.

MacDougall, J.D., Finkel, R.C., Carlson, J., Krishnaswami, S., 1979. Isotopic evidence for uranium exchange during low-temperature alteration of oceanic basalt. Earth Planet Sc Lett 42, 27–34. https://doi.org/10.1016/0012-821x(79)90187-0.

Maher, K., DePaolo, D.J., Christensen, J.N., 2006. U–Sr isotopic speedometer: fluid flow and chemical weathering rates in aquifers. Geochim Cosmochim Ac 70, 4417–4435. https://doi.org/10.1016/j.gca.2006.06.1559.

Maher, K., DePaolo, D.J., Lin, J.C.-F., 2004. Rates of silicate dissolution in deep-sea sediment: in situ measurement using ^{234}U/^{238}U of pore fluids. Geochim. Cosmochim. Acta 68, 4629–4648. https://doi.org/10.1016/j.gca.2004.04.024.

Matthews, K.A., Murrell, M.T., Goldstein, S.J., Nunn, A.J., Norman, D.E., 2010. Uranium and thorium concentration and isotopic composition in five glass (BHVO-2G, BCR-2G, NKT-1G, T1-G, ATHO-G) and two powder (BHVO-2, BCR-2) reference materials. Geostand. Geoanal. Res. 35, 227–234. https://doi.org/10.1111/j.1751-908x.2010.00080.x.

Mervine, E.M., Humphris, S.E., Sims, K.W.W., Kelemen, P.B., Jenkins, W.J., 2014. Carbonation rates of peridotite in the Samail Ophiolite, Sultanate of Oman, constrained through ^{14}C dating and stable isotopes. Geochim Cosmochim Ac 126, 371–397. https://doi.org/10.1016/j.gca.2013.11.007.

Mervine, E.M., Sims, K.W.W., Humphris, S.E., Kelemen, P.B., 2015. Applications and limitations of U–Th disequilibria systematics for determining ages of carbonate alteration minerals in peridotite. Chem. Geol. 412, 151–166. https://doi.org/10.1016/j.chemgeo.2015.07.023.

Mills, R.A., Dunk, R.M., 2010. Tracing low-temperature fluid flow on ridge flanks with sedimentary uranium distribution. Geochem. Geophys. Geosystems 11. https://doi.org/10.1029/2010gc003157 n/a-n/a.

Müller, R.D., Sdrolias, M., Gaina, C., Roest, W.R., 2008. Age, spreading rates, and spreading asymmetry of the world's ocean crust. Geochem. Geophys. Geosystems 9. https://doi.org/10.1029/2007gc001743 n/a-n/a.

Musić, S., Ristić, M., 1988. Adsorption of trace elements or radionuclides on hydrous iron oxides. J. Radioanal. Nucl. Chem. 120, 289–304. https://doi.org/10.1007/bf02037344.

Niu, Y., 2004. Bulk-rock major and trace element compositions of abyssal peridotites: implications for mantle melting, melt extraction and post-melting processes beneath Mid-Ocean Ridges. J. Petrol. 45, 2423–2458. https://doi.org/10.1093/petrology/egh068.

Paulick, H., Bach, W., Godard, M., Hoog, J.C.M.D., Suhr, G., Harvey, J., 2006. Geochemistry of abyssal peridotites (Mid-Atlantic Ridge, 15°20′N, ODP Leg 209): implications for fluid/rock interaction in slow spreading environments. Chem. Geol. 234, 179–210. https://doi.org/10.1016/j.chemgeo.2006.04.011.

Peters, D., Bretscher, A., John, T., Scambelluri, M., Pettke, T., 2017. Fluid-mobile elements in serpentinites: constraints on serpentinisation environments and element cycling in subduction zones. Chem. Geo. 466, 654–666. https://doi.org/10.1016/j.chemgeo.2017.07.017.

Pope, E.C., Bird, D.K., Rosing, M.T., 2012. Isotope composition and volume of Earth's early oceans. Proc. Natl. Acad. Sci. USA 109, 4371–4376. https://doi.org/10.1073/pnas.1115705109.

Power, I.M., Wilson, S.A., Dipple, G.M., 2013. Serpentinite carbonation for CO_2 sequestration. Elements 9, 115–121. https://doi.org/10.2113/gselements.9.2.115.

Ragan, D.M., 1963. Emplacement of the twin sisters dunite, Washington. Am. J. Sci. 261, 549–565. https://doi.org/10.2475/ajs.261.6.549.

Reyss, J.L., Lemaitre, N., Bonté, P., Franck, D., 1987. Anomalous ^{234}U/^{238}U ratios in deep-sea hydrothermal deposits. Nature 325, 798–800. https://doi.org/10.1038/325798a0.

Richter, S., Eykens, R., Kühn, H., Aregbe, Y., Verbruggen, A., Weyer, S., 2010. New average values for the n(238U)/n(235U) isotope ratios of natural uranium standards. Int. J. Mass spectrom. 295, 94–97. https://doi.org/10.1016/j.ijms.2010.06.004.

Salters, V.J.M., Stracke, A., 2004. Composition of the depleted mantle. Geochem., Geophys., Geosystems 5. https://doi.org/10.1029/2003 gc000597 n/a-n/a.

Santschi, P.H., Bajot, C., Mantovani, M., Orciuolot, D., Cranston, R.E., Bruno, J., 1988. Uranium in pore waters from North Atlantic (GME and Southern Nares Abyssal Plain) sediments. Nature 331, 155–157. https://doi.org/10.1038/331155a0.

Schlüter, M., Steuber, T., Parente, M., Mutterlose, J., 2008. Evolution of a Maastrichtian–Paleocene tropical shallow-water carbonate platform (Qalhat, NE Oman). Facies 54, 513–527. https://doi.org/10.1007/s10347-008-0150-8.

Scott, S.R., Sims, K.W.W., Frost, B.R., Kelemen, P.B., Evans, K.A., Swapp, S.M., 2017. On the hydration of olivine in ultramafic rocks: implications from Fe isotopes in serpentinites. Geochim Cosmochim Ac 215, 105–121. https://doi.org/10.1016/j.gca.2017.07.011.

Snow, J.E., Dick, H.J.B., 1995. Pervasive magnesium loss by marine weathering of peridotite. Geochim Cosmochim Ac 59, 4219–4235. https://doi.org/10.1016/0016-7037(95)00239-v.

Spivack, A.J., Edmond, J.M., 1987. Boron isotope exchange between seawater and the oceanic crust. Geochim. Cosmochim. Acta 51, 1033–1043. https://doi.org/10.1016/0016-7037(87)90198-0.

Staudigel, H., Plank, T., White, B., Schmincke, H., 1996. Subduction: Top to Bottom, Volume 96 Geochemical Fluxes During Seafloor Alteration of the Basaltic Upper Oceanic Crust: DSDP Sites 417 and 418, in: Bebout, G.E., Scholl, D.W., Kirby, S.H., Platt, J.P. (Eds.), Subduction. pp. 19–38. doi:10.1029/gm096p0019.

Stirling, C.H., Andersen, M.B., Potter, E.K., Halliday, A.N., 2007. Low-temperature isotopic fractionation of uranium. Earth Planet. Sci. Lett. 264, 208–225. https://doi.org/10.1016/j.epsl.2007.09.019.

Stirling, C.H., Halliday, A.N., Porcelli, D., 2005. In search of live ^{247}Cm in the early solar system. Geochim Cosmochim Ac 69, 1059–1071. https://doi.org/10.1016/j.gca.2004.06.034.

Tissot, F.L.H., Chen, C., Go, B.M., Naziemiec, M., Healy, G., Bekker, A., Swart, P.K., Dauphas, N., 2018. Controls of eustasy and diagenesis on the ^{238}U/^{235}U of carbonates and evolution of the seawater (^{234}U/^{238}U) during the last 1.4Myr. Geochim. Cosmochim. Acta. https://doi.org/10.1016/j.gca.2018.08.022.

Tissot, F.L.H., Dauphas, N., 2015. Uranium isotopic compositions of the crust and ocean: age corrections, U budget and global extent of modern anoxia. Geochim. Cosmochim. Acta 167, 113–143. https://doi.org/10.1016/j.gca.2015.06.034.

Tissot, F.L.H., Ibanez-Mejia, M., Boehnke, P., Dauphas, N., McGee, D., Grove, T.L., Harrison, T.M., 2019. U-238/U-235 measurement in single-zircon crystals: implications for the Hadean environment, magmatic differentiation and geochronology. J. Anal. At. Spectrom. 34, 2035–2052. https://doi.org/10.1039/c9ja00205g.

Wang, X., Planavsky, N.J., Reinhard, C.T., Hein, J.R., Johnson, T.M., 2016. A Cenozoic seawater redox record derived from ^{238}U/^{235}U in ferromanganese crusts. Am. J. Sci. 316, 64–83. https://doi.org/10.2475/01.2016.02.

Weyer, S., Anbar, A.D., Gerdes, A., Gordon, G.W., Algeo, T.J., Boyle, E.A., 2008. Natural fractionation of ^{238}U/^{235}U. Geochim. Cosmochim. Acta 72, 345–359. https://doi.org/10.1016/j.gca.2007.11.012.

Yager, J.A., West, A.J., Corsetti, F.A., Berelson, W.M., Rollins, N.E., Rosas, S., Bottjer, D.J., 2017. Duration of and decoupling between carbon isotope excursions during the end-Triassic mass extinction and Central Atlantic Magmatic Province emplacement. Earth Planet. Sci. Lett. 473, 227–236. https://doi.org/10.1016/j.epsl.2017.05.031.